Hybridization of ellipsometry and XPS energy loss: Robust band gap and broadband optical constants determination of SiGe, HfON and MoOx thin films

Théo Levert [a,*], Alter Zakhtser [a], Julien Duval [b], Chloé Raguenez [b], Stéphane Verdier [b], Delphine Le Cunff [b], Jean-Hervé Tortai [a], Bernard Pelissier [a]

[a] *Univ. Grenoble Alpes, CNRS, LTM, Minatec campus, Grenoble, France*
[b] *STMicroelectronics, Crolles, France*

ARTICLE INFO

ABSTRACT

In this study, we compare the robustness of optical constants and optical band gap determination of three different materials: SiGe, N-doped HfO_2 and MoO_x, using the combination of two techniques: spectroscopic ellipsometry, and energy loss signal (ELS) of X-ray photoelectron spectroscopy (XPS). The determination of such physical properties is achieved through the hybridization of the two techniques based on multiple Tauc-Lorentz model, applied on the whole energy range of measurement.

Such use of hybridized data demonstrates a new robust method to determine the band gap of the studied materials, together with the optical indices (refractive index and extinction coefficient) on a wide energy range (up to 40 eV). This method provides an extension of determination of the relevant physical quantities compared to each technique on their own.

Moreover, this algorithm is tested on limit conditions, where the energy ranges of measurement of the two respective techniques presented no overlap. Yet the use of a unique physical model still allows us to calculate the different physical quantities even on the energy range where no measurement is performed, validating the semi-predictive nature of the hybrid technique. Additional measurements under different experimental configurations validate the extended scope of such hybrid technique.

1. Introduction

A growing number of materials for microelectronics industry are currently under development, to benefit from unique properties, such as low band gap (SiGe), low-k (HfO2). Actors of microelectronics industry need reliable and robust metrology techniques that provide full required dimensional information of these materials. However, there is no technique that can provide such information on its own, and commonly sets of characterization techniques are adopted to get the maximum information by merging the information of each technique. For instance, critical dimension (CD) information can be obtained by ellipsometry [1], small angle x-ray scattering [2] (CD-SAXS), X-ray Reflectometry [3] (XRR), scatterometry [4], etc. but every technique comprises its own advantages and limitations, depending on the studied material or structure. Metrology plays an important role in every step of fabrication and development of microelectronics devices. With the number of

applications involved in microelectronics, a various number of techniques and components have been developed, and thus the complexity of metrology control that goes hand in hand. Technical difficulties are ranging from the characterization of complex alloys to the characterization of multiple stacks of materials, or ultra-thin materials. We are currently shifting the objective from miniaturization goal to a "more than Moore" goal with integration of digital and non-digital functions on the same chip. Thus, it leads to the development of new complex structures and materials to achieve such a goal, with many technical challenges, keeping a focus on robustness and accuracy of the measurements.

To face this challenge, ellipsometry have been intensively used as a major technique for the determination and control of the thickness and the optical constants of thin layers deposited at each step of the process. Ellipsometry is an optical technique based on the measurement of change of polarization state of light after reflection on the studied

---

sample [5]. Its strength is the non-destructive nature and its broad applications in terms of thickness (from a fraction of monatomic layers to few micrometers thick films). This technique is mainly used for thickness measurement of films, optical constants determination, but can also be used to study other properties, such as roughness, optical anisotropy, crystalline state, atomic composition, or band gap. However, this technique is model dependent and does not directly measure those parameters. Thus, the accuracy on the physical quantities, such as band gap energies, which stands as a key parameter in this study, are highly dependent on the quality of the model, and on the accuracy and the robustness of the fit. All the foreseen metrics are determined by inverse problem solving (i.e., minimizing the error between the experimental and the modeled signatures), leading to uncertainty on the final calculated value (Mean square error, local minimum, inaccurate physical model and so on). Moreover, the target band gap value should be preferentially in the range of measurement (0.6–6.5 eV for conventional ellipsometer), to reduce the uncertainty generated by the extrapolation of the material behavior outside the energy range of measurement.

X-ray Photoelectron Spectroscopy (XPS) is also a noticeable surface analysis technique used in various applications, such as photovoltaics [6], nanomaterials [7], oxides, batteries [8], or microelectronics. It is based on the study of emitted photoelectrons of a surface, induced by X-ray photons. It is mainly used for atomic identification and quantification. With recent development of angular resolved systems, it can reveal additional information, such as depth dependence or thickness of ultra-thin film [9]. Moreover, XPS can be used for the valence band and band gap determination, especially for low-k materials. It can be achieved by studying the onset of energy loss signal (ELS) after a main peak, as described by Nichols et al. [10]. This band gap determination method is based on the relation between the photoelectron emission and the energy loss signal from electrons with the same energy, which finds similarities with reflection electron energy loss technique [11–13]. However, this technique suffers from technical limitations, such as the analysis depth (<10 nm), and the difficulties of the evaluation of low target values of band gap, due to the impact of the broad main peak width.

In this study, the main idea is to benefit from the advantage of both ellipsometry and XPS techniques and to combine them in a single specific model for reliable and robust determination of physical quantities of interest, such as band gap and thickness, along with refractive index n and extinction coefficient k. This is mainly based on the direct relation of ELS with the optical constants [14]. This relation helps us to connect the two measurement techniques through a unique and continuous physical model. This technique allows a better band gap determination when compared to each technique on their own. Indeed, band gap determination from XPS suffers from unreliability, and ellipsometry suffers from uncertainty when studying large band gap materials, the measurement range being limited. The combination of the two respective techniques allows to considerably reduce those uncertainties. We previously reported the use of such model to obtain band gap energies of SiON thin films [15]. Here we report its use on three practical cases: SiGe, HfON, and MoO$_x$ materials, with broad target band gap values, ranging from 1 to 5.5 eV. Thus, we demonstrate the various range of materials that can be studied thanks to our hybrid model. We discuss the advantages and drawbacks of the use of the hybrid model in terms of robustness and accuracy depending on the material studied. Indeed, it seems that the hybrid model does not have a strong impact when applied to determination low band gap materials, whereas it appears to highly reduce the uncertainties of wide band gap determination. Moreover, we compared the determined values of band gap and/or thickness with conventional techniques to demonstrate its reliability and robustness. Regarding the refractive index and extinction coefficient, the hybrid technique allows a new simple way of determination on a wide energy range. Finally, the variety of materials pointed out different technical limitations for each case. Despite those technical difficulties, the hybrid model appeared to still stand as a powerful method.

2. Material and methods

2.1. Material growth

Concerning the epitaxial growth of SiGe, in total 5 samples were epitaxially grown on 300 mm silicon wafers using reduced-Pressure Chemical Vapor Deposition (RPCVD). Firstly, Si wafers were cleared from their native oxide with a 1050 °C annealing at partial pressure. Then the epitaxy was performed under selected temperature ranging from 600 to 700 °C, with selected partial pressures of H$_2$SiCl$_2$, HCl and GeH$_4$ to achieve various composition of Si and Ge.

One HfO$_2$ sample and three N-doped HfO$_2$ (HfON) samples were grown on 300 mm silicon wafers. HfON samples were elaborated in a 3-steps sequence. First, HfO$_2$ layer is deposited by ALD on a PULSAR ASM chamber. Then, a plasma nitridation followed by an annealing at 600 °C is performed in an Applied Materials Centura tool. All tools are industrial 300 mm tools.

MoO$_x$ thin film sample was deposited by PVD (Physical Vapor Deposition) from Mo metallic target. MoO$_x$ stoichiometry could vary by changing the oxygen flow used during the deposition.

2.2. Experimental techniques

XPS and ellipsometry spectroscopy measurements were performed on the full set of samples using different facilities from LTM and STMicroelectronics to assess and validate the use of the determination technique on variable experimental tools.

XPS has been carried out on a Theta 300 from Thermo Scientific on the IMPACT platform of LTM and STMicroelectronics on a VeraFlex II from Nova under ultra-high vacuum conditions (10^{-9} and 10^{-7} mbar respectively), both alongside an X-ray source of Al K$\alpha_{1,2}$ with a photon energy of 1486.6 eV.

For the SiGe samples, we collected the photoelectrons from the Si2p and Ge3d regions. Those two regions were used for elemental quantification, and the Ge3d peak was used for the collection of energy loss signal.

For the HfON samples, we collected the photoelectrons from the Hf4f, Hf4d, O1s and N1s regions. It should be emphasized that the Hf4f region was used for the elemental quantification, and that the Hf4d region was collected in a wide energy range (from 190 to 270 eV) for the collection of the energy loss function.

For the MoO$_x$ samples, the photoelectron energy regions of Mo3d (from 380 to 460 eV) and O1s (from 525 to 575 eV) were collected. These two regions were processed for both element quantification and study of the energy loss signal.

Ellipsometry measurements were performed with a VUV spectroscopic (phase modulated) ellipsometer UVISEL2 from Horiba on IMPACT characterization platform with a fixed angle of incidence of 70° and an extended energy range of 0.6–8 eV under vacuum conditions (5 10^{-3} mbar). The scanning configuration of the instrument was set with an analyzer at 45° and a modulator angle of 0°. The same measurements were performed with a SpectraFilm LD10 from KLA (rotating analyzer), with a fixed angle of incidence of 64.9° with a standard range of 0.6–6 eV.

The two different facilities were based on different requirements. The LTM facility is more "lab-oriented", with a spectroscopic ellipsometer in a vacuum chamber, whereas the STMicroelectronics ellipsometer is an in-line metrology facility under atmospheric pressure. This also applies for the two XPS, with different pressure of measurements (10^{-9} and 10^{-7} mbar for LTM and STMicroelectronics respectively), or different flux level. Those differences were an opportunity to demonstrate the ability of the hybrid model to be used on both facilities, which validates its use in microelectronics industry.

The different measurements were performed on the same points, around the center of the wafers, between LTM and STMicroelectronics facilities for consistency purpose.

Note that the raw data measured by the UVISEL are the physical quantities *Is* and *Ic*, whereas the raw data measured by the LD10 are the cosine and sine Fourier coefficients α and β, which are equivalent and linked through the following relations [16]:

$$Is = sin(2\Psi).sin(\Delta)$$

$$Ic = sin(2\Psi).cos(\Delta)$$

$$\alpha = \frac{tan^2(\Psi) - tan^2(P)}{tan^2(\Psi) + tan^2(P)}$$

$$\beta = \frac{2tan(P).tan(\Psi).cos(\Delta)}{tan^2(\Psi) + tan^2(P)}$$

With Ψ and Δ the ellipsometric angles, related to the Fresnel coefficient r_p and r_s:

$$\rho = \frac{r_p}{r_s} = tan(\Psi).e^{i\Delta}$$

and P being the azimuth of the polarizer. An example of measured ellipsometric quantities *Is* and *Ic* using LTM equipment on HfO₂/Si sample can be found in Fig. 1. It must be pointed out that the small shift at around 1.2 eV is attributed to the backside reflection of the Si substrate around its band gap, due to its transparent behavior below band gap.

After having defined a stack of materials, as presented for instance in Fig. 2, with each stack having its own optical indices and thickness (optical indices coming from either reference data e.g. for the substrate, or modeled for the studied material), we can calculate the physical quantities of interest (*Is*, *Ic* or α, β depending on the equipment) with the help of the Fresnel equations. This allows the comparison of modeled physical quantities with raw measurements for adjustment of the parameters.

As stated before, the raw measurements cannot be converted directly to the optical constants of the studied material and thus require the use of a physical model which will be described in detail in the next section.

2.3. Calculation: Tauc-Lorentz based hybrid model

Optical index of material can be modeled using dispersion laws, preferred ones being those who respect Kramer-Kronig relations that insure a physically relevant law.

The Tauc-Lorentz (TL) model is a physically relevant semi-empirical dispersion law that was developed by Jellison and Modine [17] to model the dielectric function of materials. It is based on the combination of the Tauc density of state [18] and a Lorentz oscillator [19]. It is commonly used to describe the optical properties of a broad range of semiconductor materials and polymers. It offers the advantage of considering the band
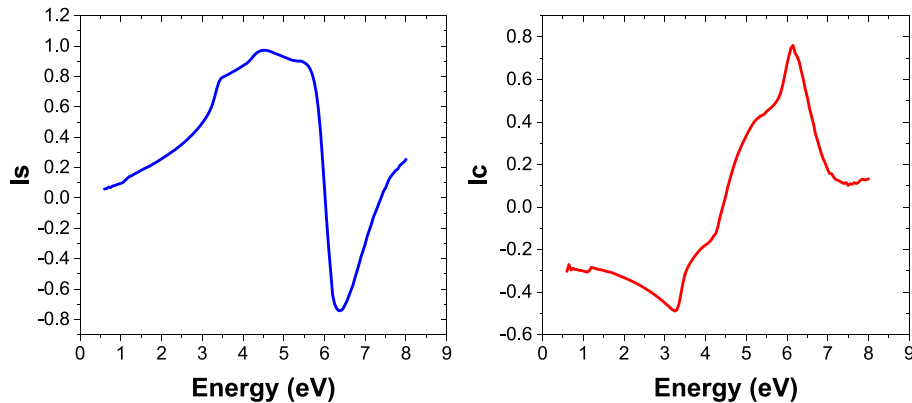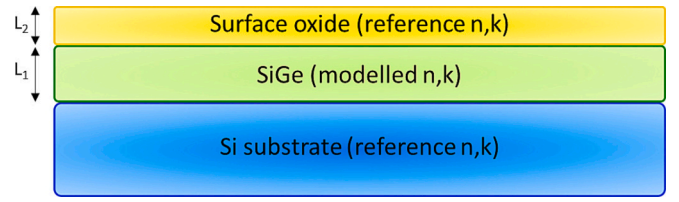

Fig. 2. Example of materials stack to consider for ellipsometry calculation.

gap of semiconductor materials, which stands as a key parameter in this study. It can be described by the following expressions:

$$\widetilde{\varepsilon}_{TL} = \varepsilon_{r,TL} + i.\varepsilon_{i,TL} = \varepsilon_{r,TL} + i.\left(\varepsilon_{i,T} \times \varepsilon_{i,L}\right)$$

With $\varepsilon_{i,TL}$ the imaginary part of the dielectric function given by the product of the Tauc density of state $\varepsilon_{i,T}$ and the Lorentz dielectric part $\varepsilon_{i,L}$ which can also be described as:

$$\varepsilon_{i,T}\left(E > E_g\right) = A_T.\left(\frac{E - E_g}{E}\right)^2$$

where A_T is the Tauc coefficient, E is the photon energy, E_g is the optical band gap. This imaginary part of the Tauc's dielectric function gives the response of the material caused by inter-band mechanism, thus $\varepsilon_{i,T}\left(E \leq E_g\right) = 0$.

The imaginary part of the Lorentzian oscillator model is described as:

$$\varepsilon_{i,L}(E) = \frac{A_L.E_0.C.E}{\left(E^2 - E_0^2\right)^2 + C^2.E^2}$$

where A_L is the strength parameter of the peak, C the broadening parameter, E_0 the central energy peak.

When using N-oscillator Tauc-Lorentz model, the dielectric constant. $\varepsilon = \varepsilon_r + i.\varepsilon_i$ is then defined by its imaginary part:

$$\varepsilon_i(E) = \begin{cases} \sum_{i=1}^{N}\frac{1}{E}.\frac{A_i.E_i.C_i\left(E - E_g\right)^2}{\left(E^2 - E_i^2\right)^2 + C_i^2 E^2} & for\ E > E_g \\ 0\ for\ E \leq E_g \end{cases}$$

Where

$$A_i = A_{T,i} \times A_{L,i}.$$

What stands out from the Tauc-Lorentz model is that its permittivity is Kramers-Kronig consistent, due to the causality of the system, which is not the case of all models frequently used in ellipsometry.

Thus the real part of the dielectric constant ε_r is obtained from the imaginary part of the dielectric constant ε_i using the Kramers-Kronig relation [16]:

Fig. 1. Is and Ic measured by LTM facilities on HfO₂ sample.

$$\varepsilon_r(E) = \varepsilon_r(\infty) + \frac{2}{\pi} . P . \int_{E_g}^{\infty} \frac{\xi . \varepsilon_i(\xi)}{\xi^2 - E^2} d\xi$$

where P is the Cauchy principal value which contains the residues of the integral, since the integrands diverge for $E = \xi$ and $\varepsilon_r(\infty)$ is the real permittivity of the material at low frequencies. This integral yields to an analytical solution developed by Jellison and Modine [17] which is beyond the scope of this paper and will not be described here. From this description, we can calculate the real part of the dielectric constant numerically.

It can be noted that for an N-oscillator model, the number of parameters used to describe the dielectric constant is $2 + 3.N$ which correspond to $\varepsilon_r(\infty)$, E_g, and $N \times (A_i, E_i, C_i)$ to which the thickness parameter must be added in the Fresnel calculation.

From the evaluation of the real and imaginary part of the dielectric constant, one can obtain the refractive index and extinction coefficient through the relations:

$$n^2 = \frac{1}{2}\left(\varepsilon_r + \sqrt{\varepsilon_r^2 + \varepsilon_i^2}\right) \text{ and } k^2 = \frac{1}{2}\left(-\varepsilon_r + \sqrt{\varepsilon_r^2 + \varepsilon_i^2}\right)$$

Ellipsometry signatures will be calculated using those optical indices. Fresnel equations and Snell-Descartes law are used to generate the calculation of the physical quantities relevant to the ellipsometry tools, i.e., Is, Ic or α, β depending on the equipment. In this purpose a multiple stack of films is considered, depending on the studied structure. In our case the studied films being deposited on silicon substrate, the stack consists of the substrate, the thin layer of interest, in some case a thin oxide layer and/or in some case and a thin roughness layer, as described for instance in Fig. 2. The roughness layer can be optically modeled by optical constants derived from a mixture of 50–50% of void and the studied material, with the help of Bruggeman effective medium approximation [20], which is commonly used to take into account the contribution of roughness in the total reflected light in ellipsometry [21].

XPS can be used for approximate band gap determination, by considering the onset of the ELS after a main peak by linear regression of the ELS, as previously described [10,15]. We can see an example of band gap determination with this method on Fig. 3 on SiON samples. However, this method presents some limitations, such as the accuracy of the band gap values, which is highly dependent on the quality (broadening) of the main XPS peak. Consequently, for low band gap materials, such as SiGe, this method appeared to be very inaccurate, and thus were not employed.
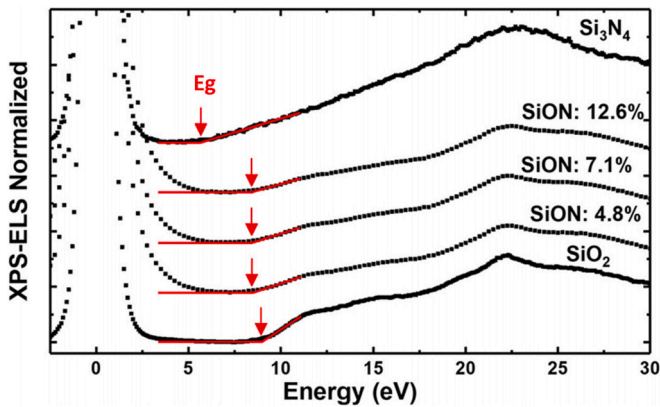
Energy loss signal is directly induced by plasmon generation, and thus by the electric field of incident electrons. As a result, energy loss signal is related to the dielectric constant of the material, and is expressed by:

$$ELS = Im\left(\frac{-1}{\varepsilon}\right)$$

Which leads, regarding n and k, to:

$$ELS = \alpha \frac{2.n.k}{\left(n^2 + k^2\right)^2}$$

Experimentally, the ELS obtained from XPS measurements are normalized regarding the maximum of the signal. An example of ELS experimental data can be found in Fig. 4, acquired from the Ge3d peak of an SiGe sample. We can also see that the minimum after the main peak, i. e., the starting point of the ELS, is directly dependent on the broadening of the main XPS peak. Indeed, a larger peak would lead to a higher energy starting point and thus to less information on the low energy of the ELS. After normalization, a form factor α has been introduced to take into consideration the uncertainties of such a normalization, and to allow the use of a continuous model from the lower energies (from the ellipsometry measurement) to higher energies (from ELS), with or without overlap, for consistency. The value of α is set as a parameter for consistency between the two types of datasets and to compensate the possible uncertainty of the background line of the ELS spectra. Moreover α values are systematically around 1 and does not vary much for a set of material.

The physical quantities relevant to the problem- (Is, Ic, ELS) or (α, β, ELS) depending on the equipment being calculated through the different relations stated before, an inverse problem-solving algorithm has been developed to adjust the different parameters, so the experimental data fit the simulated data. It has been achieved through the use of Python numpy and lmfit libraries [22,23].

3. Results and discussion

3.1. Epitaxial SiGe

$Si_{(1-x)}Ge_x$ materials, denoted as SiGe materials are studied in this section. In total, 5 different samples are presented, with a Ge content varying from 9.1 to 30.2%, as determined by ellipsometry calibrated on
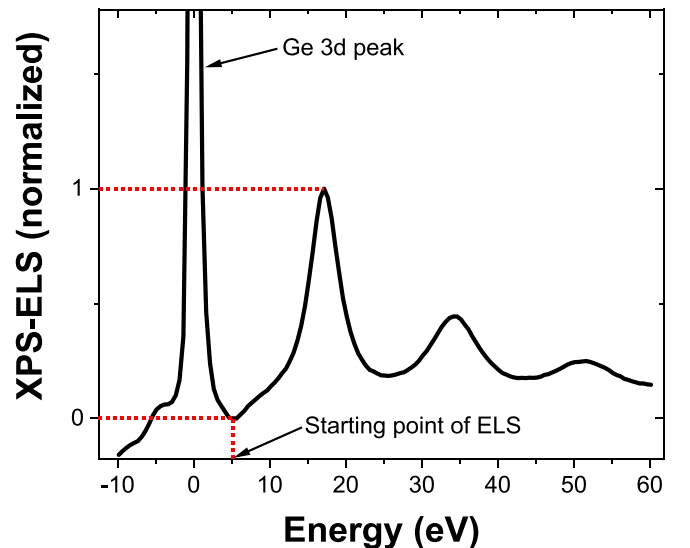

Fig. 3. XPS-ELS experimental data after the main peak for the SiO2–Si3N4 thin films. All spectra represent the ELS after the O1s main core peak, except the Si3N4 where the N1s ELS is pictured. Red lines represent the horizontal baseline and the linearization of the threshold energy from ELS. Red arrows show the energy value of the determined band gap. From ref. [15]. (For interpretation of the references to colour in this figure legend, the reader is referred to the web version of this article.)

Fig. 4. XPS-ELS experimental data acquired on SiGe sample from the onset of the Ge3d peak.

XRD measurements (STMicroelectronics model, not detailed here), and thicknesses ranging from 18 to 23 nm, as determined by the hybrid model. A surface oxide layer was also considered for the calculation of the model. The stack has been schematized on Fig. 5.

In this case the Ge incorporation plays an important role in band gap engineering, as well as optical constants variation, which turns the use of the hybrid modeling as an essential tool for robust determination of relevant physical quantities. In this purpose ellipsometry measurements were performed on all samples on both facilities (LTM and STMicroelectronics) with respective energy ranges of measurements of 0.6–8 and 0.6–6 eV respectively. Energy loss signal was extracted from the Ge 3d peak of each sample. The method of evaluation of the band gap from the onset of XPS-ELS, as previously employed for other materials [10,15], and as discussed in the material and method section, was not suitable in our case due to narrower band gap materials. Indeed, expected band gap values are between the range of Ge and Si band gap (0.67–1.14 eV respectively), making the use of such method tough, due to experimental parameters, such as the width of the main peak, and thus was not employed here.

The hybrid model has been employed on the combination of ellipsometric quantities *Is* and *Ic* along with the ELS from Ge 3d peak. For the inverse problem solving, a total of 10 TL oscillators were used on the energy range of combined techniques (0.6–40 eV). Indeed regarding the ellipsometry part, we started our investigation by modeling the optical indices of pure Si with reference data from Jellison [24], based on Tauc-Lorentz oscillators. It appeared that a total of 7 TL oscillators were necessary to obtain reasonable modeled optical constants to fit the reference data, as one can see on Fig. 6. Then, three additional TL oscillators were employed in the hybrid model to consider the impact of the ELS part of the dataset, leading to a total of 10 TL oscillators. The final sets of parameters used for the fitting process of the different thin films can be found in supplementary material.

One can see the comparison of ellipsometric quantities *Is* and *Ic* coming from the raw measurements of LTM facilities (scatters), along with the result of the fit from the hybrid model (solid lines), stacked for visual purpose for the different samples of various Ge concentration. (See Fig. 7).We can observe the very good agreement between the measured data and the fitted ones, as well as the slight evolution of the curves with the addition of Ge in the films. The resulted $\chi 2$ values were in the range 0.13–0.23 for the ellipsometry energy range, with $\chi 2$ defined as:

$$\chi^2 = \frac{1}{N_{ellipso}} \left(\sum_{j=1}^{N_{ellipso}} \frac{(I_S^{model} - I_S^{exp})2}{\sigma_{Is}^2} + \sum_{j=1}^{N_{ellipso}} \frac{(I_c^{model} - I_c^{exp})2}{\sigma_{Ic}^2} \right)$$

Moreover, we presented the ELS spectra coming from measurement (from Ge3d peak) along with the ELS coming from the same single hybrid modeling, for the 9.1% Ge sample on Fig. 8. We can see the good agreement between the two curves, confirming the robustness of the model.

Since the band gap E_g is a parameter of the model, we are able to determine its value. For our five samples, the band gap values have been calculated with the use of the hybrid model and compared with values determined by ellipsometry alone. We can see the associated band gap values on Fig. 9. The uncertainty of band gap values has been estimated around 0.02 eV (based on the relation between the band gap variation and the ellipsometry quantities Is variation, determined experimentally

as 5.10^{-3}). We also presented on the same figure the reported values by Lang et al. [25] of strained and unstrained SiGe. We can see the band gap values are closer to the reported strained values for the hybrid model method, which is coherent with the epitaxial growth of our samples. This seems to show that the hybrid model presents more accuracy compared to ellipsometry on its own. However, the calculated values of band gaps are close to values determined by ellipsometry only, and thus the use of the hybrid model does not have a major impact on the calculation of the band gap in this case. Indeed, the expected band gap values are quite low (1–1.11 eV), and then the use of additional TL oscillators outside the range of ellipsometry measurement, beyond 8 eV (i. e., in the range of ELS measurement) does not have a strong impact on the determined band gap values. Yet the band gap is only one parameter of the model and even the hybrid model does not add a strong value to its determination in low band gap materials, we can see the reliability of its use when compared to ellipsometry on its own.

The hybrid model plays an important role in optical constants determination. We were able to determine the refractive index and extinction coefficient on the whole energy range of combined techniques (i.e., 0.6–40 eV) for all samples. We presented on Fig. 10 an example of n and k determination on the whole range of measurement of combined techniques. Additionally we presented on Fig. 11 a comparison of optical constants determined by the hybrid model for all samples, along with reference data of Si and Ge from Jellison [24,26]. We focused the graph on ellipsometry range (0.6–8 eV) for visual purpose, but one can remember the modeled optical constants were determined on the whole energy range of combined techniques, as presented for the 9.1% Ge sample on Fig. 10. On Fig. 11, we can see the good agreement and tendencies of the optical constants with Ge incorporation. Very similar results were obtained using STMicroelectronics measurements and thus were not shown here, but this information confirms the robustness of the hybrid model, giving around the same set of parameters, regardless of the experimental configuration of the measurements.

Moreover, we can find on Table 1 the determined thicknesses of the different SiGe thin films determined by XRR, ellipsometry alone and the hybrid model. It revealed firstly that the thickness determined by ellipsometry or the hybrid model are very close, which indicates that the hybrid model does not has a major impact on the thickness determination. Secondly, the thickness determined by XRR are systematically slightly higher than the two other methods, but still consistent. This slight bias could be attributed to the influence of the substrate, the film interfaces, inaccurate values of optical constants of the film, or inaccurate determination of roughness top layer of the structure.

Finally, we were able to characterize the physical quantities of interest with the help of our hybrid model. Such model provides a reliable determination of parameters such as band gap or thickness of the films. However, its use with low band gap materials such as SiGe revealed no major difference compared to ellipsometry only. This can be explained by the fact that addition of information far beyond the band gap does not influence much the value of the determined band gap, the XPS-ELS being at high energies. Moreover, the use of the hybrid model allows determination of the refractive index and extinction coefficient on a wide energy range of combination of the two techniques (i.e., 0.6–40 eV), through the use of a unique, consistent and continuous model on the whole range of measurement.

3.2. HfON

In total, four samples have been studied. One reference sample of pure HfO_2 with a thickness of 8 nm and three samples of N-doped HfO_2 (HfON), denoted as Wafer 1–3, with different nitrogen content, and a target thickness of 2 nm, as determined by the hybrid model. An additional roughness layer has been considered on the top of HfON to best evaluate its physical response. This roughness layer was optically modeled by optical constants derived from a mixture of 50–50% of void
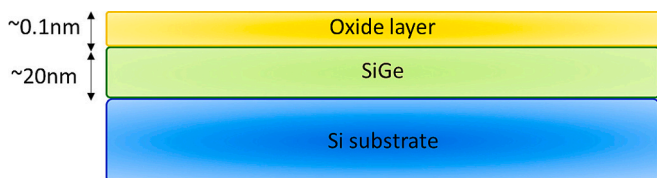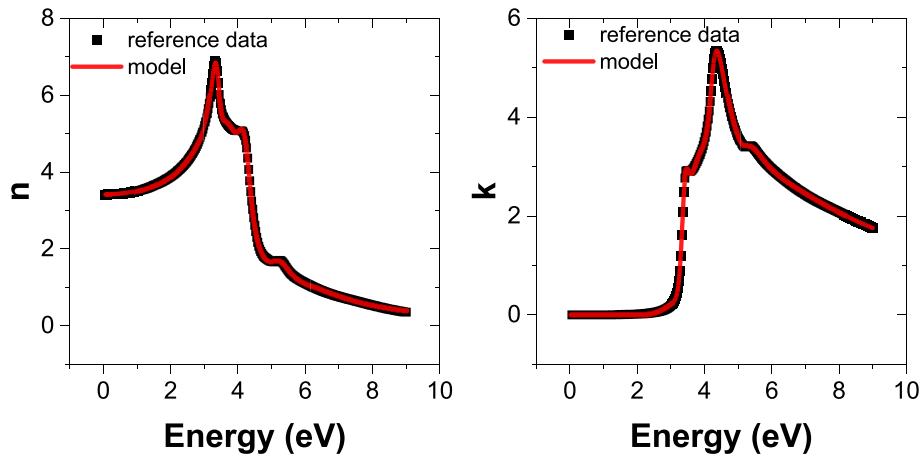

Fig. 5. Schematic view of SiGe samples stack.

Fig. 6. Refractive index and extinction coefficient of crystalline Silicon from Jellison [24], and from the 7TL model.
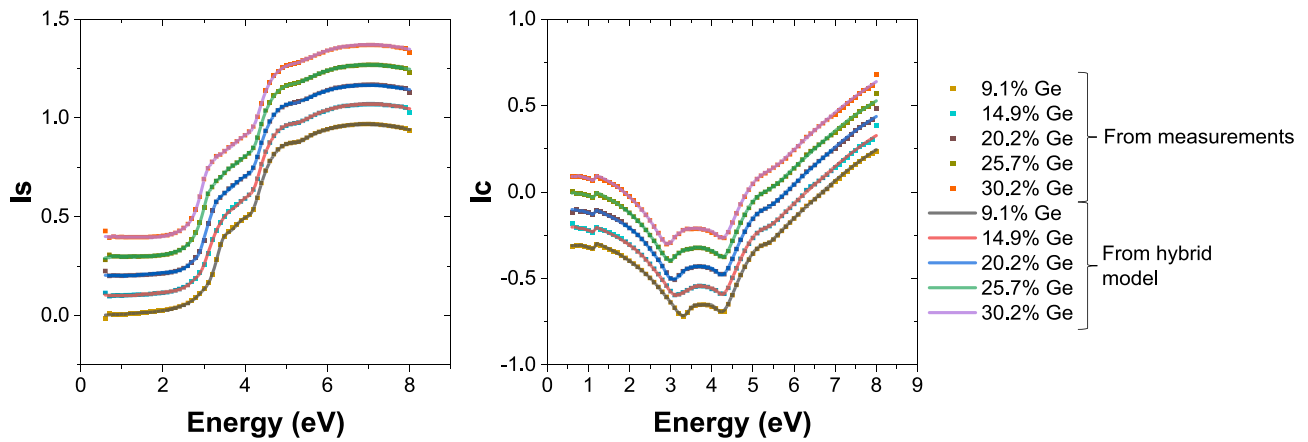

Fig. 7. Comparison of a) Is and b) Ic for the different samples, from the raw measurements of LTM facilities and the hybrid model.
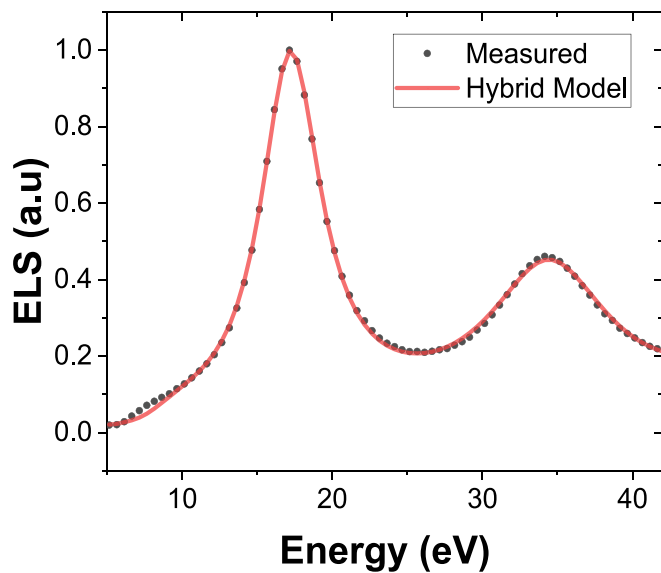

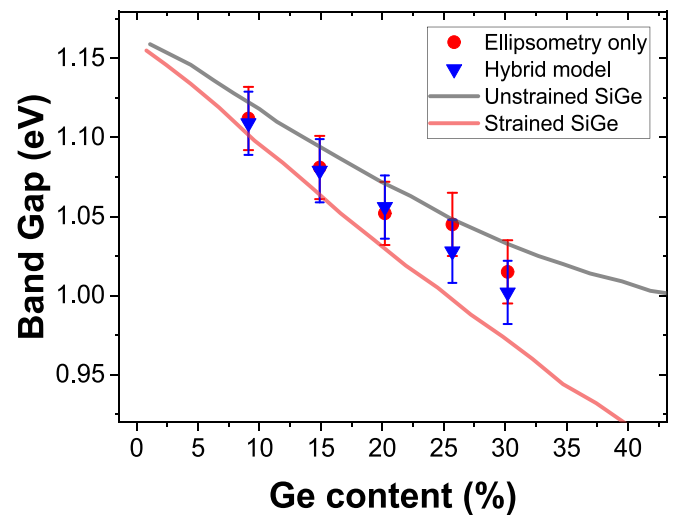**Fig. 8.** ELS spectra from measurement and hybrid model for Ge3d peak.

Fig. 9. Comparison of band gap values determined by the hybrid model and by ellipsometry only with LTM data, along with reported values of strained and unstrained SiGe from ref. [25].

and the studied material, with the help of Bruggeman effective medium approximation [20]. An example of the stack of the samples can be found in Fig. 12.

Classical XPS analysis helped us to estimate the nitrogen con-

tent N/(Hf + O + N) which was 5.26, 9.46 and 13.05% for the three doped samples (Wafer 1–3 respectively). The thicknesses of the films were also evaluated from ARXPS measurement with values between 20.47 and 21.80 Å for the HfON samples. The method of evaluation of
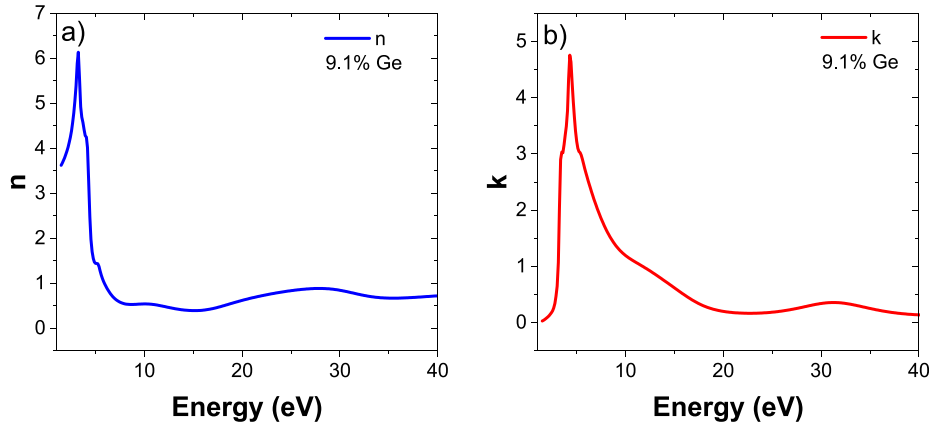
Fig. 10. Refractive index *n* and extinction coefficient *k* determined by the hybrid model with LTM data on wide energy range for the 9.1% Ge sample.
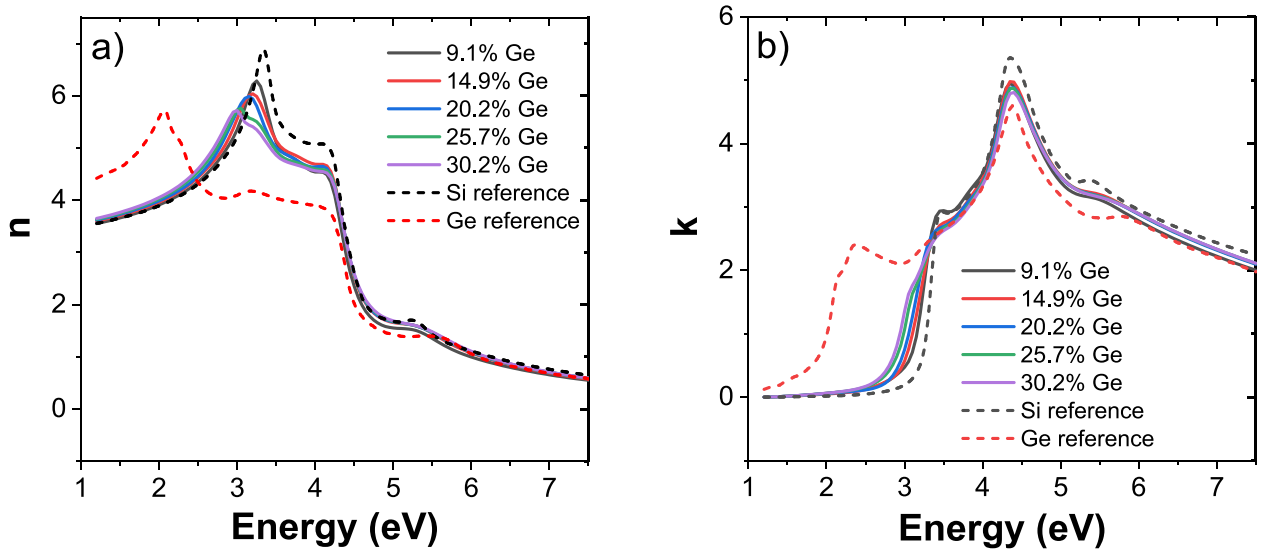

Fig. 11. Comparison of a) refractive index *n* and b) extinction coefficient *k* determined from the hybrid model with the Ge content using LTM data. We presented for visual comparison the n and k of Si and Ge only from reference [24, 26] respectively.

Table 1
Thickness of SiGe thin films, determined by XRR, ellipsometry and hybrid model using LTM data.

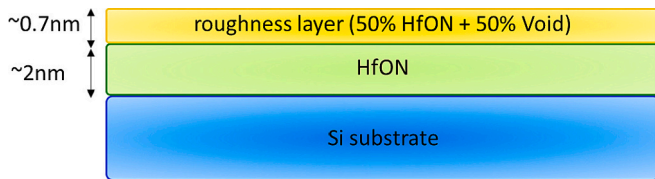| Wafer n°	% Ge	Thickness XRR (nm)	Thickness Ellipsometry (nm)	Thickness Hybrid model (nm)
13	9.1	27.19571	23.1	19.98
15	14.9	20.03582	18.3	18.07
16	20.2	21.59971	20.4	20.34
17	25.7	20.59529	20.1	20.14
14	30.2	21.94982	19.7	19.06

Fig. 12. Schematic view of HfON samples stack.

the band gap from XPS-ELS, as discussed in the material and method section, and as previously employed for other materials [10,15], was not suitable in our case due to narrower band gap materials. Indeed, the minimum values predicted with this direct method were far beyond expected band gap values of such materials. Hf4d peak of XPS was chosen for the extraction of the ELS, its binding energy position not overlapping with other peaks in a reasonable range after the main peaks.

The main physical quantities of ellipsometry *Is* and *Ic* were collected on the two characterization platforms with different energy ranges: 0.6–6.5 eV on STMicroelectronics side, and 0.6–8 eV on LTM side. For each sample, the hybrid model was employed in combination with the ELS from the Hf4d peak of XPS (on either LTM or STMicroelectronics facilities), using these two sets of data, in order to validate the use of the model with a reasonable energy range of prediction, where no data were collected. In this purpose, three Tauc-Lorentz oscillators were used to fit the experimental data, giving a total set of 13 parameters (3 per oscillator, ε_∞, E_g, α and the thickness of the film). Indeed, the number of necessary Tauc-Lorentz oscillators was obtained using reference HfO_2 data. It appeared that 3 TL oscillators were sufficient to model the full energy range of ellipsometry and ELS. The final sets of parameters used for the fitting process of the different thin films can be found in supplementary material.

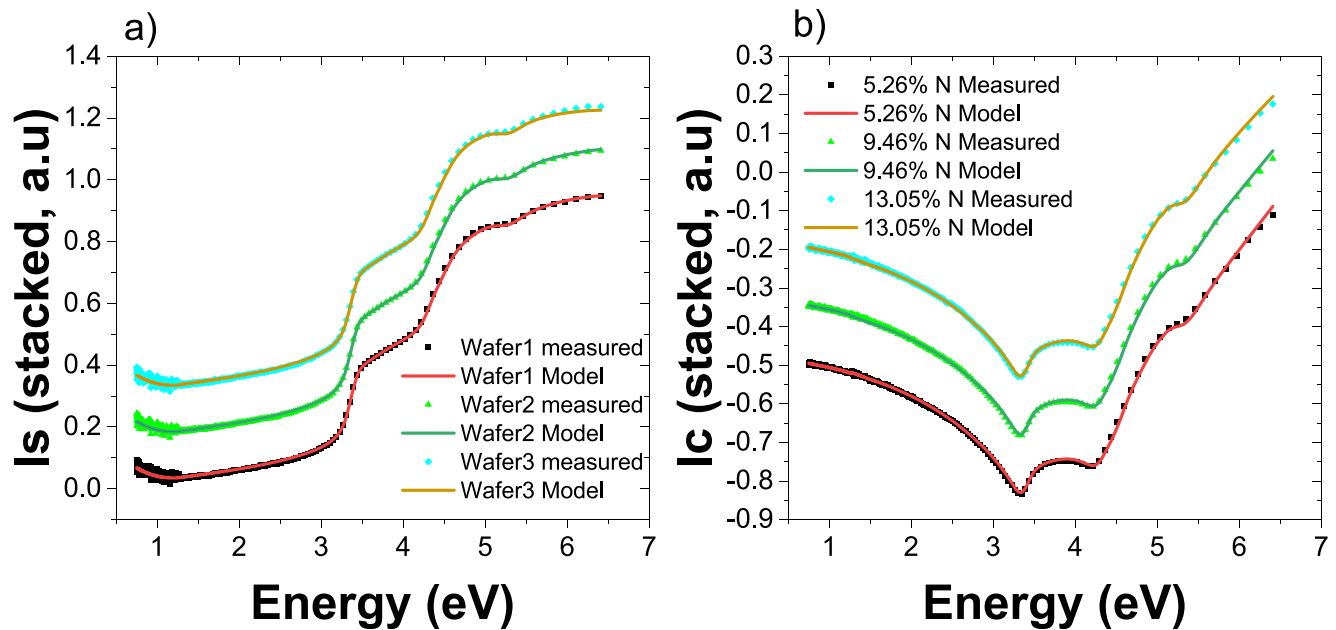One can find on Fig. 13 the result of the fit of *Is* and *Ic* using the

Fig. 13. Comparison of a) *Is* and b) *Ic* for the three different samples, from the raw measurements of ST facilities and the hybrid model.

hybrid model with the energy range measurement of STMicroelectronics equipment (0.6–6.5 eV). We can notice the very good agreement between the experimental data (dots) and modeled data (lines) for the three different samples, with resulting $\chi 2$ values below 0.1 for all datasets.

The reference sample was not shown here for visual purpose, its thickness and thus its signature being different from the three doped samples (around 10 nm), but the same model was also performed on associated data. The model was else performed on the LTM data with an energy range of measurements of 0.6–8 eV, producing in the same way a very good agreement between measurements and modeled data (not shown here) with resulting $\chi 2$ values also below 0.1 for all data.

Resulting from the same modeling, we presented on Fig. 14 the ELS measured with the fitted curve of the two datasets (STMicroelectronics and LTM) with the different energy ranges on the 5.26% N sample. Concerning the fitted curves (solid lines), different colors are presented to visually identify the different ranges of measurements between the two facilities, keeping in mind that for each curve, a unique and continuous physical solution of the problem is obtained from the model. Here we can clearly identify the "blind" energy range, where no measurement was performed between the two techniques on each curve. For the LTM measurements, this "blind" energy range is only 0.3 eV whereas it is around 4.6 eV for the STMicroelectronics measurements. This difference of energy range is directly due to the different experimental setup. Indeed, the LTM ellipsometry measurements were performed up to 8 eV whereas they were performed up to 6.5 eV using STMicroelectronics ellipsometer. Also, the broadenings of the main XPS peaks were different using the two facilities, leading to a larger blind energy range using the STMicroelectronics facilities. Despite this difference, the model performed on the two datasets delivered very similar results.

For the band gap values, which is a key parameter in this study, Fig. 15 shows the band gap values determined by the hybrid model on the STMicroelectronics and LTM datasets, along with band gap values determined by ellipsometry only (only STMicroelectronics data were
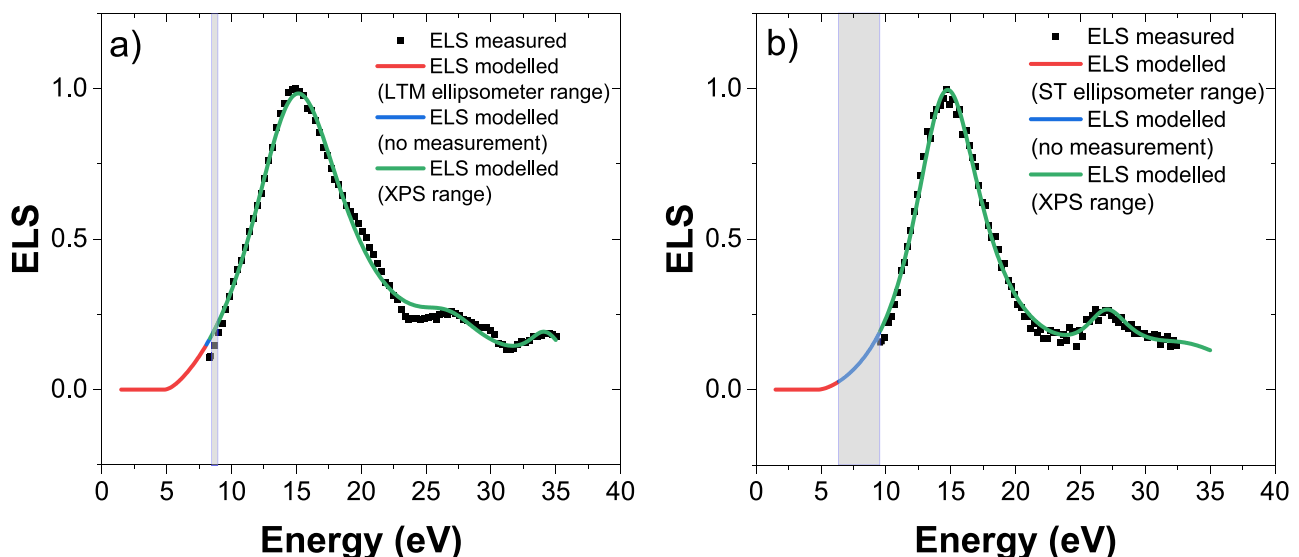

Fig. 14. Comparison of ELS measurement and modeled data using a) LTM data and b) ST data on the 5.26% N sample.
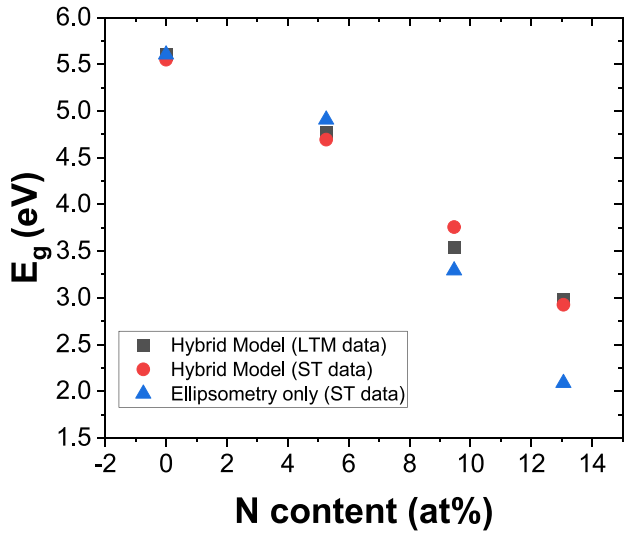
Fig. 15. Comparison of band gap values determined by the hybrid model with the use of ST data, LTM data, and values determined by ellipsometry only using ST data.

presented here for visual comfort).

On one hand, we can observe the very good agreement between the two datasets where the hybrid model was performed, and, on the other hand, we can observe the slight differences of the band gap values between the hybrid model and the ellipsometry model alone. The first point is a major information on the extended use of the hybrid model, since we can validate its use, even with a reasonable "blind" energy range between the two respective techniques, where no measurements were performed. The slight differences between the hybrid model and the ellipsometry alone tend to diverge with the N content increase. This underestimation using ellipsometry only may be due to excitonic absorption with low energy tails, related to defects in materials and/or the indirect character of such material [27]. These results showed consistency with previously reported values of band gap with nitrogen incorporation for low concentration [28]. However for higher nitrogen content, the band gap values appeared to be lower than other few studies [29–31]. This difference can be explained by the different process of nitrogen incorporation, or the thin film quality. The tendency of this variation seems consistent with electronic theory. Indeed, the conduction band minimum in pure HfO_2 is due to non-bonding Hf5d states, whereas its valence band maximum is due to O2p states. Incorporating N adds N2p state, resulting in a shift of the valence band maximum, with a maximum rise of around 2.6 eV for the maximum doping level of nitrogen for the sample 3. Thus, the model allows a robust determination of key parameters such as band gap.

Moreover, the hybrid model provides a determination of the optical

constants (refractive index n and extinction coefficient k) on a wide energy range (0.6–35 eV), as presented in Fig. 16. It shows a consistent variation of the optical indices with the incorporation of nitrogen, and primarily a robust determination on a wide energy range, which is, in the case of HfON, a key information, since measurements using classical ellipsometry only enables a determination up to 6 eV, which is at a point of great variation of optical constants, as one can realize on Fig. 16.

3.3. MoO_x

3.3.1. Hybrid model on MoO_x

An additional case was explored with MoO_x materials, using a 300 mm wafer of 14.6 nm thickness, as determined by the hybrid model. The thin film was deposited on Si substrate, and a roughness top layer was considered, to best evaluate its physical response. An example of the considered stack can be found in Fig. 17.

Classical XPS, with consideration of the Mo3d and O1s peaks, helped us to determine the atomic ratio of oxygen and molybdenum $O/(O + Mo)$ in the films which was found to be 73.47%, letting us considerate a little oxygen deficient MoO_3.

Moreover, the binding energy positions of the two main peaks of Mo3d were found to be 232.6 and 235.74 eV for Mo $3d_{5/2}$ and Mo $3d_{3/2}$ respectively, which is in good agreement of previous reported values for Mo(VI) for MoO_3 [32–34]. Additionally, we investigated the possible presence of other valence state of molybdenum, here Mo(V) and Mo(IV), by fixing the binding energy positions of such peaks according to reported values in literature [32–34] of those possible states. After close inspection, the possible presence of such states is anecdotal, since their identification is below sensitivity of XPS. We cannot exclude their presence completely, but analysis of the spectrum let us consider molybdenum to be mainly in Mo(VI) state.

ELS spectrum were extracted from O1s and Mo3p peaks of XPS, in order to assess and validate the use of the hybrid model on signals collected from the two species of MoO_x sample.

Ellipsometry measurements were performed on the sample again with energy ranges of 0.6–6 eV and 0.6–8 eV using the two different facilities of STMicroelectronics and LTM respectively. The hybrid model was applied with the two different ELS spectra, giving four different use cases. The hybrid model was based on the use of four Tauc-Lorentz
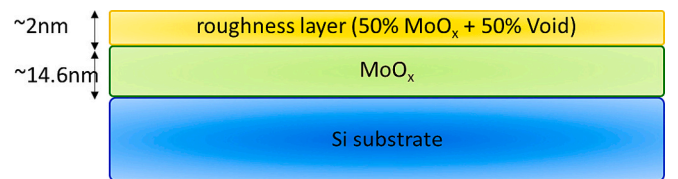

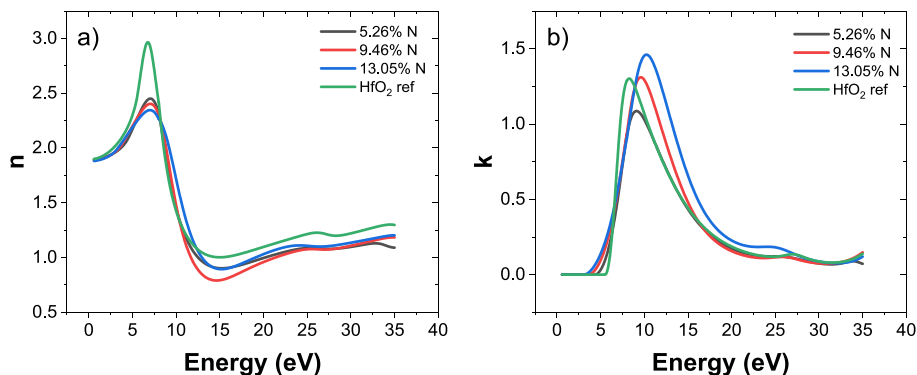**Fig. 17.** Schematic view of MoO_x samples stack.

Fig. 16. a) Refractive index n and b) extinction coefficient k of the HfON and reference HfO_2 thin films obtained from the hybrid model using ST dataset.

oscillators, and an additional Lorentz oscillator centered on the near-infrared region to consider the sub-gap absorption of such films. This sub-gap absorption has already been reported and studied [35,36], and can be ascribed to a small polaron, a quasiparticle characterized by the interaction of a trapped electron with atoms in the surrounding area [37,38], which is frequently observed for transition metal oxides.

All different datasets presented similar results, with a maximum variation of the determined band gap of around 0.02 eV, along with a maximum variation of the determined thickness of the film of around 0.27 nm. These results indicate the robustness of the hybrid model, considering the very small variation of relevant parameters such as band gap or thickness of the thin film, with the use of different experimental datasets, acquired on different equipment systems, with different experimental configurations.

One can find on Fig. 18 an example of the modeled ellipsometric quantities *Is* and *Ic* with the use of the hybrid model, along with the experimental data from LTM facilities (energy range of 0.6–8 eV). Thus, we can observe a very good agreement between the model and the experimental data, with a resulting $\chi 2$ below 0.1 for all ST datasets and below 0.35 for all LTM datasets, on the ellipsometry range. This difference between the two types of datasets should reasonably be attributed to uncertainties in the experimental acquisition, especially on UV region using LTM facilities, leading to a higher $\chi 2$, and shouldn't be attributed to uncertainties of the mathematical minimization, since the parameters determined by the hybrid model are very close between the two datasets.

One should pay close attention to the ELS spectrum determined by the hybrid model using the distinct datasets. Indeed, we collected the ELS from two main peaks of the XPS: Mo3p and O1s. Thus, experimental parameters such as broadening of the peak or the range of measurements without any disturbance leads to different ELS spectra, as we can see on Fig. 19. We can clearly see the starting point of the ELS spectrum differs from Mo3p to O1s, with a starting point of 7.9 eV for the ELS coming from the Mo3p peak, and 4.6 eV for the ELS coming from the O1s peak. As one can see this little difference of energy of 3.3 eV deprived the ELS of Mo3p of an additional peak, that can be clearly identified in the ELS of O1s.

Despite this discrepancy, and since the hybrid model is carried out on the energy range of the combination of ellipsometry and ELS through a unique and continuous physical modeling, we can clearly see the very good agreement of the modeled ELS along with the experimental data, between the distinct datasets, using either ellipsometry data of LTM (0.6–8 eV) or STMicroelectronics (0.6–6 eV), and either ELS from Mo3p or O1s. The final sets of parameters used for the fitting process of the MoO$_x$ thin film based on the different datasets can be found in supplementary material. These results allow us to state on the high robustness and accuracy of the use of such hybrid modeling.

Moreover, the refractive index *n* and extinction coefficient *k* were
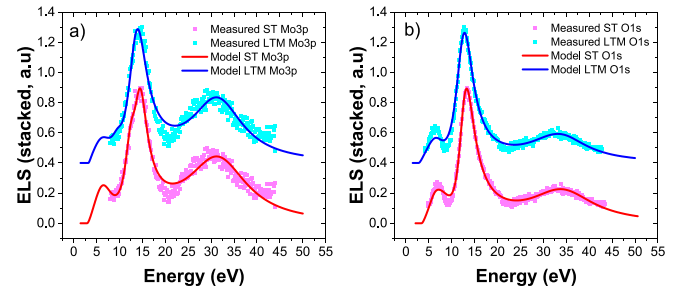

Fig. 19. Comparison of ELS from measurements and hybrid model with ST and LTM facilities, using ELS from a) Mo3p and b) O1s main peak.

determined with the help of the hybrid model either LTM and STMicroelectronics data, with the help of ELS coming from either Mo3p or O1s peak. All determined values of *n* and *k* were found to be very similar. We presented on Fig. 20 the determined values over a wide energy range, for the hybrid model using LTM data with ELS from O1s as an example. We can clearly see the good consistency with reported values of Vos et al. [39] over their range of measurement. Furthermore, we can see the great interest of using the hybrid model for *n* and *k* determination, since additional oscillations are described beyond the range of conventional ellipsometry measurement, allowing us to access their values via the use of the model.

3.3.2. Mapping on MoO$_x$

Additionally, the hybrid model was employed on full-wafer scale, with the help of mapping consisting of 17 points of measurement on the 300 mm wafer. The idea was to validate the use of such model for in-line metrology manufacturing and to demonstrate the high accuracy and robustness of such method. Thus, the hybrid model was successively
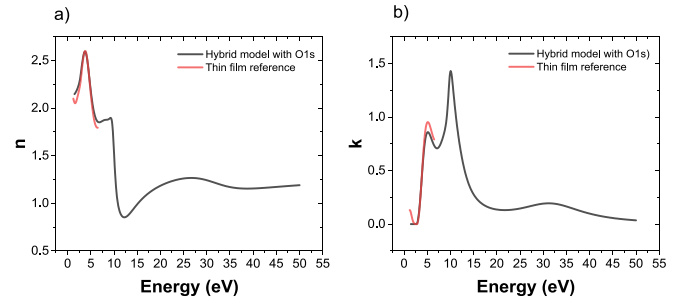

Fig. 20. a) Refractive index *n* and b) extinction coefficient *k* determined by the hybrid model with the ELS from O1s peak, along with determined values from reference [39].
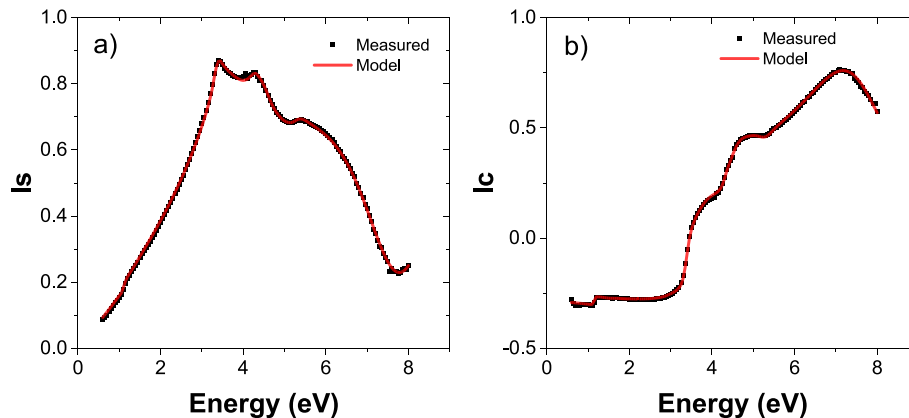

Fig. 18. Comparison of a) *Is* and b) *Ic* from measurement and hybrid model, using LTM dataset.

applied to the 17 points of measurements, using either ELS from Mo 3p or O 1 s, and the different parameters resulting from the inverse problem-solving algorithm were extracted for each point of measurement and each ELS. For instance, we presented a wafer mapping of the thickness of the MoO$_x$ thin film in Fig. 21. The rough thickness extracted from the hybrid model on different points were extrapolated using the Thin Plate Spline (TPS) algorithm in order to build the thickness profile on the whole wafer level, as we can observe on Fig. 21. We can see the high correlation of determined thickness using ELS from Mo 3p and O 1 s spectrum, as previously discussed on a single point. Moreover, we compared the thickness determined with the help of our hybrid model with the thickness determined by X-ray Reflectometry (XRR) measurements on Fig. 21.c), performed on the same 17 points. The resulting thickness mapping is in very good agreement with the hybrid model, using either Mo 3p or O 1 s ELS. Finally, we presented on Fig. 21.d) the point-by-point thickness determined by the three different types of determination method (hybrid model with Mo3p ELS, hybrid model with O1s ELS, and XRR). We can put the spotlight on two main information:

- First, we can observe that the determined thickness using the hybrid model (either using Mo3p or O1s ELS), were systematically slightly higher than using XRR measurements (1-2 Å). This small offset between XRR and our hybrid model have been reported in numerous studies concerning XRR and ellipsometry [40–45], and thus could be attributed to the influence of the substrate, the film interfaces, inaccurate values of optical constants of the film, or inaccurate determination of roughness top layer of the structure.
- Despite this small offset, we can observe the high correlation of the determined thickness when compared with the hybrid model and XRR measurement point by point, confirming the high robustness of the hybrid model, with Pearson's correlation coefficients of 0.954

and 0.921 for the XRR along with the hybrid model with Mo3p or O1s ELS respectively.

Finally, we demonstrated the ability of our hybrid model to be employed on a whole 300 mm wafer level, which presents great advantages for metrology control of critical physical quantities, such as the thickness of the film.

We also calculated the band gap of the MoO$_x$ on the same 17 points of measurements using the hybrid model, with the help of the two types of ELS (Mo3p or O1s). We presented on Fig. 22 the band gap mapping resulting from the hybrid model. This emphasizes first the same tendencies of the band gap variation across the wafer, along with a high accuracy on band gap determination. Indeed, we obtained a mean band gap value of 2.753 eV with a standard variation of 0.0307 eV for the dataset with Mo3p ELS, and a mean band gap value of 2.756 eV with a standard variation of 0.0261 eV for the dataset with O1s ELS, which is close to the determined band gap by ellipsometry only with a value of 2.751 eV. Although we do not have additional measurements to corroborate those band gap values, the very low standard variations and very similar mean values of band gap demonstrate the high reliability of such method.

4. Conclusion

In conclusion, we demonstrate the robustness and reliability of our hybrid model through its use in various cases. First the hybrid has been applied to the SiGe case, where the measurement data presented an overlap between the two respective techniques. We were able to determine physical quantities of interest, such as band gap and thickness of the different samples, with reliability. This was achieved through the use of a single continuous physical model on the whole range of measurements of combined ellipsometry and ELS. Moreover, we were able to get
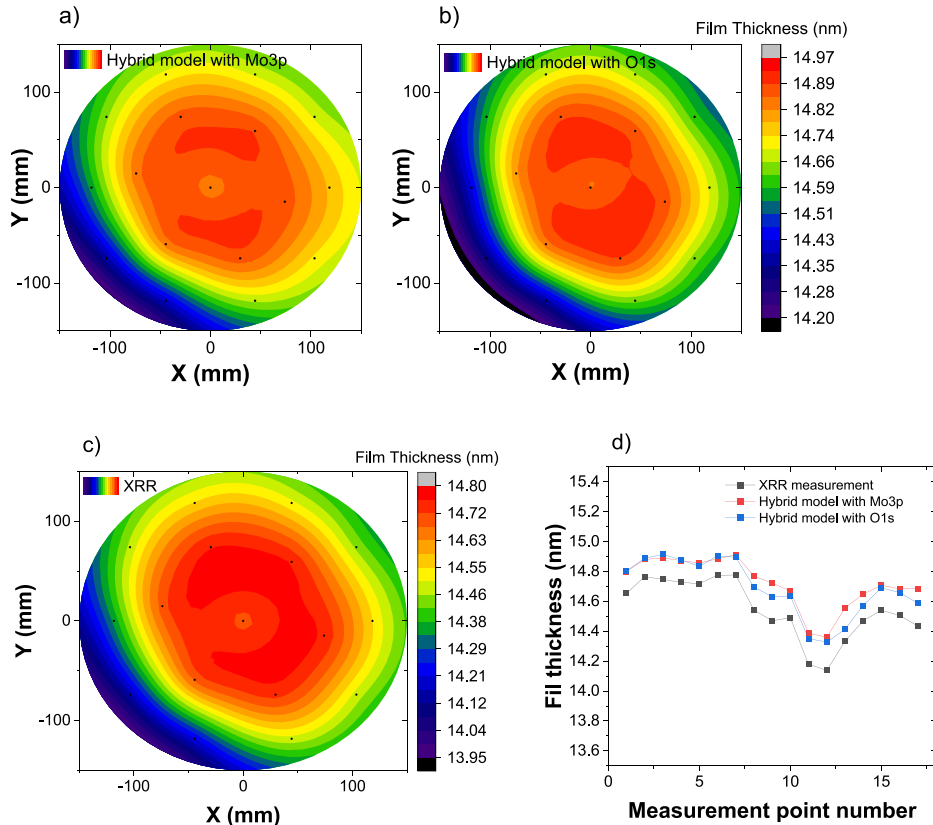

Fig. 21. Thickness mapping at wafer level of MoO$_x$ sample, using the hybrid model with ELS from a) Mo3p and b) O1s main peaks. c) Thickness mapping using XRR measurement. d) point by point comparison of thickness coming from a)-c).
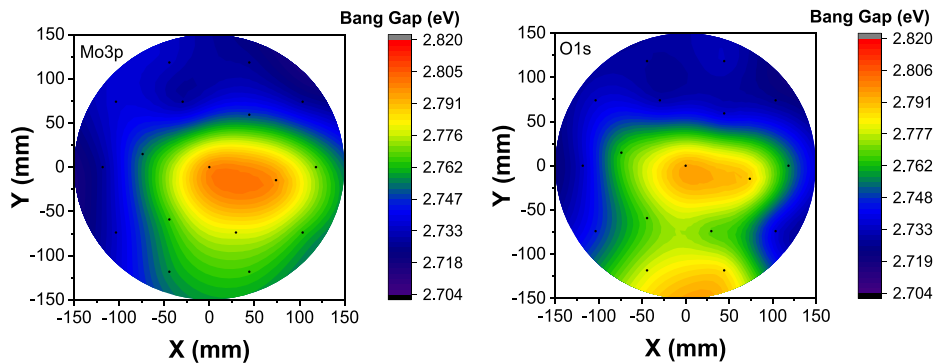
Fig. 22. Band gap mapping of MoO_x 300 mm wafer determined by the hybrid model with ELS collected from Mo3p and O1s.

a determination of the optical constants over a wide energy range, scaling from 0.6 to 40 eV. However, the hybrid model presented no major advantages on the band gap determination when compared to other techniques (e.g., ellipsometry only), due to low band gap values (around 1 eV). Nevertheless, the hybrid model proved its ability for optical constants determination over a wide energy range, demonstrating a simple way to access the refractive index and extinction coefficient, especially outside energy range of conventional techniques such as ellipsometry alone. We believe this hybridization technique is only an example of what could be achieved with advanced data analysis of physical properties. Here we demonstrated a simple way to determine the optical constants beyond the energy range of measurement of ellipsometry.

We validated the use of the hybrid model firstly with SiGe materials. It appeared that the hybrid model didn't have a strong impact on the determination of the band gap, since SiGe present low band gap value. Indeed, the addition of information by ELS, with high energy does not influence the low value of the determined band gap (~1 eV). Though, the hybrid model presented a great advantage of the determination of the optical constants over the wide energy range of measurements of the combined techniques, demonstrating a simple way to access such information, with techniques compatible with microelectronics industry.

We applied our hybrid model on HfON case, using facilities from LTM and STMicroelectronics, leading to a blind energy range between the two techniques, where no data were collected (due to technical limitations). Despite those blind energy ranges (0.3 eV for LTM and 4.6 eV for STMicroelectronics), the physical quantities of interest extracted from the hybrid models were noticeably the same, demonstrating the robustness of the hybrid model. Then we can validate its use with a reasonable blind energy range between the two techniques.

Then MoO_x material has been studied, with the help of LTM and STMicroelectronics facilities, in combination with ELS spectrum from two different main peaks of XPS, leading to a total of four datasets. In all cases, the hybrid model revealed similar physical quantities of interest. The use of different ELS spectra did not influence either the determined parameters (band gap, thickness…) or the evaluation of optical constants. Those observations are validating again the robustness of the hybrid model. Additionally, mapping measurements were carried out on 300 mm wafer using in-line facilities of STMicroelectronics. We compared the reconstructed thickness surface with XRR measurements, which showed a high degree of correlation, validating the use of the hybrid model for industrial metrology systems.

Finally, we demonstrated the high reliability and robustness of a hybrid model based on combination of ellipsometry and XPS-ELS, through the use of a unique and continuous model through the energy range combination of the two respective techniques, based on TL oscillators. It must be pointed out that the two facilities are experimentally different, with the LTM one more "lab-oriented", with measurement under vacuum for the ellipsometry part, whereas the ST one is an in-line metrology tool. This difference exposed the validity of the hybrid model

on different experimental setups and validates its use in microelectronics industry. We highlighted the high accuracy of such model for critical physical quantities determination such as thin film thickness or band gap. We set out its easy way of optical indices determination over a wide energy range (up to 40 eV). Finally, we demonstrated its use in an industrial metrology environment for future in-line control.

CRediT authorship contribution statement

Théo Levert: Writing – original draft, Methodology, Software. **Alter Zakhtser:** Investigation, Resources. **Julien Duval:** Investigation, Resources. **Chloé Raguenez:** Investigation, Resources. **Stéphane Verdier:** Investigation, Resources. **Delphine Le Cunff:** Investigation, Resources, Supervision, Project administration. **Jean-Hervé Tortai:** Writing – review & editing, Software, Methodology. **Bernard Pelissier:** Writing – review & editing, Methodology, Supervision, Project administration.

Declaration of Competing Interest

None.

Data availability

The data that has been used is confidential.

Appendix A. Supplementary data

Supplementary data to this article can be found online at https://doi.org/10.1016/j.mee.2023.112117.

References

[1] H.-T. Huang, F.L. Terry Jr., Spectroscopic ellipsometry and reflectometry from gratings (Scatterometry) for critical dimension measurement and in situ, real-time process monitoring, Thin Solid Films 455–456 (2004) 828–836, https://doi.org/10.1016/j.tsf.2004.04.010.

[2] T. Hu, R.L. Jones, W. Wu, E.K. Lin, Q. Lin, D. Keane, S. Weigand, J. Quintana, Small angle x-ray scattering metrology for sidewall angle and cross section of nanometer scale line gratings, J. Appl. Phys. 96 (2004) 1983–1987, https://doi.org/10.1063/1.1773376.

[3] K.N. Stoev, K. Sakurai, Review on grazing incidence X-ray spectrometry and reflectometry, Spectrochim. Acta B At. Spectrosc. 54 (1999) 41–82, https://doi.org/10.1016/S0584-8547(98)00160-8.

[4] C. Raymond, Overview of Scatterometry applications in high volume silicon manufacturing, AIP Conf. Proc. 788 (2005) 394–402, https://doi.org/10.1063/1.2062993.

[5] G.E. Jellison, Data analysis for spectroscopic ellipsometry, Thin Solid Films 234 (1993) 416–422, https://doi.org/10.1016/0040-6090(93)90298-4.

[6] A. Leblanc, N. Mercier, M. Allain, J. Dittmer, V. Fernandez, T. Pauporté, Lead- and iodide-deficient (CH3NH3)PbI3 (d-MAPI): the bridge between 2D and 3D hybrid perovskites, Angew. Chem. Int. Ed. 56 (2017) 16067–16072, https://doi.org/10.1002/anie.201710021.

[7] M. d'Halluin, T. Mabit, N. Fairley, V. Fernandez, M.B. Gawande, E. Le Grognec, F.-X. Felpin, Graphite-supported ultra-small copper nanoparticles – preparation, characterization and catalysis applications, Carbon. 93 (2015) 974–983, https://doi.org/10.1016/j.carbon.2015.06.017.

[8] R. Grissa, A. Abramova, S.-J. Tambio, M. Lecuyer, M. Deschamps, V. Fernandez, J.-M. Greneche, D. Guyomard, B. Lestriez, P. Moreau, Thermomechanical polymer binder reactivity with positive active materials for Li metal polymer and Li-ion batteries: an XPS and XPS imaging study, ACS Appl. Mater. Interfaces 11 (2019) 18368–18376, https://doi.org/10.1021/acsami.9b01761.

[9] C.S. Fadley, Instrumentation for surface studies: XPS angular distributions, J. Electron Spectrosc. Relat. Phenom. 5 (1974) 725–754. http://inis.iaea.org/Search/search.aspx?orig_q=RN:7249466 (accessed May 20, 2021).

[10] M.T. Nichols, W. Li, D. Pei, G.A. Antonelli, Q. Lin, S. Banna, Y. Nishi, J.L. Shohet, Measurement of bandgap energies in low-k organosilicates, J. Appl. Phys. 115 (2014), 094105, https://doi.org/10.1063/1.4867644.

[11] T. Nagotomi, Z.-J. Ding, R. Shimizu, Derivation of new energy-loss functions as applied to analysis of Si 2p XPS spectra, Surf. Sci. 359 (1996) 163–173, https://doi.org/10.1016/0039-6028(96)00366-4.

[12] S.W. King, B. French, E. Mays, Detection of defect states in low-k dielectrics using reflection electron energy loss spectroscopy, J. Appl. Phys. 113 (2013), 044109, https://doi.org/10.1063/1.4788980.

[13] D. Tahir, S. Tougaard, Electronic and optical properties of cu, CuO and Cu2O studied by electron spectroscopy, J. Phys. Condens. Matter 24 (2012), 175002, https://doi.org/10.1088/0953-8984/24/17/175002.

[14] T. Yamamoto, A. Ohta, M. Ikeda, K. Makihara, S. Miyazaki, Evaluation of dielectric function of thermally-grown SiO2 and GeO2 from energy loss signals for XPS Core-line photoelectrons, ECS Trans. 75 (2016) 777, https://doi.org/10.1149/07508.0777ecst.

[15] J. Resende, D. Fuard, D. Le Cunff, J.-H. Tortai, B. Pelissier, Hybridization of ellipsometry and energy loss spectra from XPS for bandgap and optical constants determination in SiON thin films, Mater. Chem. Phys. 259 (2021), 124000, https://doi.org/10.1016/j.matchemphys.2020.124000.

[16] H.G. Tompkins, E.A. Irene, Handbook of Ellipsometry, 2005.

[17] G.E. Jellison, F.A. Modine, Parameterization of the optical functions of amorphous materials in the interband region, Appl. Phys. Lett. 69 (1996) 371–373, https://doi.org/10.1063/1.118064.

[18] J. Tauc, R. Grigorovici, A. Vancu, Optical properties and electronic structure of amorphous germanium, Phys. Status Solidi B 15 (1966) 627–637, https://doi.org/10.1002/pssb.19660150224.

[19] F. Wooten, Optical properties of solids, Am. J. Phys. 41 (1973) 939–940, https://doi.org/10.1119/1.1987434.

[20] D.A.G. Bruggeman, Berechnung verschiedener physikalischer Konstanten von heterogenen Substanzen. III. Die elastischen Konstanten der quasiisotropen Mischkörper aus isotropen Substanzen, Ann. Phys. 421 (1937) 160–178, https://doi.org/10.1002/andp.19374210205.

[21] D.E. Aspnes, J.B. Theeten, F. Hottier, Investigation of effective-medium models of microscopic surface roughness by spectroscopic ellipsometry, Phys. Rev. B 20 (1979) 3292–3302, https://doi.org/10.1103/PhysRevB.20.3292.

[22] C.R. Harris, K.J. Millman, S.J. van der Walt, R. Gommers, P. Virtanen, D. Cournapeau, E. Wieser, J. Taylor, S. Berg, N.J. Smith, R. Kern, M. Picus, S. Hoyer, M.H. van Kerkwijk, M. Brett, A. Haldane, J. del Río, M. Wiebe, P. Peterson, P. Gérard-Marchant, K. Sheppard, T. Reddy, W. Weckesser, H. Abbasi, C. Gohlke, T.E. Oliphant, Array programming with NumPy, Nature. 585 (2020) 357–362, https://doi.org/10.1038/s41586-020-2649-2.

[23] M. Newville, T. Stensitzki, D.B. Allen, A. Ingargiola, LMFIT: non-linear Least-Square minimization and curve-fitting for Python, Zenodo (2014), https://doi.org/10.5281/zenodo.11813.

[24] G.E. Jellison, Optical functions of silicon determined by two-channel polarization modulation ellipsometry, Opt. Mater. 1 (1992) 41–47, https://doi.org/10.1016/0925-3467(92)90015-F.

[25] D.V. Lang, R. People, J.C. Bean, A.M. Sergent, Measurement of the band gap of GexSi1−x/Si strained-layer heterostructures, Appl. Phys. Lett. 47 (1985) 1333–1335, https://doi.org/10.1063/1.96271.

[26] G.E. Jellison, Optical functions of GaAs, GaP, and Ge determined by two-channel polarization modulation ellipsometry, Opt. Mater. 1 (1992) 151–160, https://doi.org/10.1016/0925-3467(92)90022-F.

[27] R. Jinno, C.S. Chang, T. Onuma, Y. Cho, S.-T. Ho, D. Rowe, M.C. Cao, K. Lee, V. Protasenko, D.G. Schlom, D.A. Muller, H.G. Xing, D. Jena, Crystal orientation dictated epitaxy of ultrawide-bandgap 5.4- to 8.6-eV α-(AlGa)2O3 on m-plane sapphire, Sci. Adv. 7 (2021) eabd5891, https://doi.org/10.1126/sciadv.abd5891.

[28] G. Shang, P.W. Peacock, J. Robertson, Stability and band offsets of nitrogenated high-dielectric-constant gate oxides, Appl. Phys. Lett. 84 (2003) 106–108, https://doi.org/10.1063/1.1638896.

[29] Y.B. Lee, I.-K. Oh, E.N. Cho, P. Moon, H. Kim, I. Yun, Characterization of HfOxNy thin film formation by in-situ plasma enhanced atomic layer deposition using NH3 and N2 plasmas, Appl. Surf. Sci. 349 (2015) 757–762, https://doi.org/10.1016/j.apsusc.2015.05.066.

[30] H.-S. Jung, H.K. Kim, J.H. Kim, S.-J. Won, D.-Y. Cho, J. Lee, S.Y. Lee, C.S. Hwang, J.-M. Park, W.-H. Kim, M.-W. Song, N.-I. Lee, S. Heo, Electrical and Bias temperature instability characteristics of n-type field-effect transistors using HfO x N y gate dielectrics, J. Electrochem. Soc. 157 (2010) G121, https://doi.org/10.1149/1.3332778.

[31] X.J. Wang, L.D. Zhang, M. Liu, J.P. Zhang, G. He, The effect of nitrogen concentration on the band gap and band offsets of HfOxNy gate dielectrics, Appl. Phys. Lett. 92 (2008), 122901, https://doi.org/10.1063/1.2903097.

[32] P.A. Spevack, N.S. McIntyre, A Raman and XPS investigation of supported molybdenum oxide thin films. 1, Calcinat. Reduct. Stud. (2002), https://doi.org/10.1021/j100144a020.

[33] M. Diskus, O. Nilsen, H. Fjellvåg, S. Diplas, P. Beato, C. Harvey, E. van Schrojenstein Lantman, B.M. Weckhuysen, Combination of characterization techniques for atomic layer deposition MoO3 coatings: from the amorphous to the orthorhombic α-MoO3 crystalline phase, J. Vac. Sci. Technol. A 30 (2011) 01A107, https://doi.org/10.1116/1.3643350.

[34] L.D. López-Carreño, G. Benítez, L. Viscido, J.M. Heras, F. Yubero, J.P. Espinós, A. R. González-Elipe, Oxidation of molybdenum surfaces by reactive oxygen plasma and O2+ bombardment: an auger and XPS study, surface and Interface, Analysis. 26 (1998) 235–241, https://doi.org/10.1002/(SICI)1096-9918(199804)26:4<235::AID-SIA360>3.0.CO;2-A.

[35] D. Scirè, P. Procel, A. Gulino, O. Isabella, M. Zeman, I. Crupi, Sub-gap defect density characterization of molybdenum oxide: an annealing study for solar cell applications, Nano Res. 13 (2020) 3416–3424, https://doi.org/10.1007/s12274-020-3029-9.

[36] J. Liu, S. Shao, G. Fang, B. Meng, Z. Xie, L. Wang, High-efficiency inverted polymer solar cells with transparent and work-function tunable MoO3-Al composite film as cathode buffer layer, Adv. Mater. 24 (2012) 2774–2779, https://doi.org/10.1002/adma.201200238.

[37] M. Dieterle, G. Weinberg, G. Mestl, Raman spectroscopy of molybdenum oxides, Phys. Chem. Chem. Phys. 4 (2002) 812–821, https://doi.org/10.1039/B107012F.

[38] A. Gulino, G. Tabbì, CdO thin films: a study of their electronic structure by electron spin resonance spectroscopy, Appl. Surf. Sci. 245 (2005) 322–327, https://doi.org/10.1016/j.apsusc.2004.10.026.

[39] M.F.J. Vos, B. Macco, N.F.W. Thissen, A.A. Bol, W.M.M. Erwin Kessels, Atomic layer deposition of molybdenum oxide from (NtBu)2(NMe2)2Mo and O2 plasma, J. Vac. Sci. Technol. A 34 (2015) 01A103, https://doi.org/10.1116/1.4930161.

[40] A. Richter, R. Guico, J. Wang, Calibrating an ellipsometer using x-ray reflectivity, Rev. Sci. Instrum. 72 (2001) 3004–3007, https://doi.org/10.1063/1.1379603.

[41] S. Kohli, C.D. Rithner, P.K. Dorhout, A.M. Dummer, C.S. Menoni, Comparison of nanometer-thick films by x-ray reflectivity and spectroscopic ellipsometry, Rev. Sci. Instrum. 76 (2005), 023906, https://doi.org/10.1063/1.1848660.

[42] U. Karabiyik, M. Mao, S.K. Satija, A.R. Esker, Determination of thicknesses and refractive indices of polymer thin films by multiple incident media ellipsometry, Thin Solid Films 565 (2014) 72–78, https://doi.org/10.1016/j.tsf.2014.06.050.

[43] D.V. Likhachev, Evaluation of different dispersion models for correlation of spectroscopic ellipsometry and X-ray reflectometry, Rev. Sci. Instrum. 90 (2019), 023909, https://doi.org/10.1063/1.5050492.

[44] K. Hasche, P. Thomsen-Schmidt, M. Krumrey, G. Ade, G. Ulm, J. Stuempel, S. Schaedlich, W. Frank, M. Procop, U. Beck, Metrological characterization of nanometer film thickness standards for XRR and ellipsometry applications, in: Recent Developments in Traceable Dimensional Measurements II, International Society for Optics and Photonics, 2003, pp. 165–172, https://doi.org/10.1117/12.512216.

[45] S.R. Wasserman, G.M. Whitesides, I.M. Tidswell, B.M. Ocko, P.S. Pershan, J.D. Axe, The structure of self-assembled monolayers of alkylsiloxanes on silicon: a comparison of results from ellipsometry and low-angle x-ray reflectivity, J. Am. Chem. Soc. 111 (1989) 5852–5861, https://doi.org/10.1021/ja00197a054.